ISBN: 978-3-95450-238-7 ISSN: 2226-0358 doi:10.18429/JACoW-ICALEPCS2023-M02A003

THE SOLID SAMPLE SCANNING WORKFLOW AT THE EUROPEAN XFEL

A. Garcia-Tabares*, A. Kardoost, C. Deiter, L. Gelisio, S. Hauf, I. Karpics, J. Schulz, F. Shohn
European X-ray Free Electron Laser Facility GmbH, Holzkoppel 4, Schenefeld, Germany

Abstract

The fast solid sample scanner (FSSS) used at the European XFEL (EuXFEL) enables data collection from multiple samples while minimizing the need for a sample-holder exchange. To optimise scan duration, target positions can be identified in advance, thus preventing the (X-ray) exposure of empty locations. In this contribution, the automated sample delivery workflow for performing solid sample scanning using the FSSS is described. This workflow covers the entire process, from automatically identifying target positions within the sample, using machine learning algorithms, to setting the parameters needed to perform the scans. The integration of this solution into the EuXFEL control system, Karabo, not only allows to control and perform the scans with the existing scan tool but also provides tools for image annotation and data acquisition. The solution thus enables the storage of data and metadata for future correlation across a variety of beamline parameters set during the experiment.

INTRODUCTION

Fixed targets are widely used among the instruments at the European XFEL, when using the 10 Hz train repetition mode [1], instead of the MHz rate burst rate. To scan such solid samples a common hardware component, the solid sample scanner, is used at 5 out of the 7 instrumental end stations of the European XFEL. The FSSS is a device equipped with two perpendicular stepper motors, enabling precise scanning along both the X and Y axes, with Z representing the beam direction. This scanner is situated above a hexapod that regulates the distance between the sample and the in-line microscope. Samples scanned using the FSSS include foil targets, wires, structured samples or powder samples encapsulated in Kapton and ultra-thin silicon nitride membranes in microfabricated silicon chips, among others. The sample so scanned thus cover a wide range of applications.

Despite the widespread use and recent hardware advancements [2,3], preparing the sample scanner for measurements remains a time-consuming and lengthy process. Typically, this procedure involves several steps: sample loading, individual sample characterization, data collection, and post-measurement analysis.

Samples are loaded into a designated holder outside the vacuum chamber and then individually placed into the interaction chamber without breaking the vacuum. Subsequent sample characterization occurs during the nominal beam time, usually during the night, and can last between 4 to 8 hours. The data collection process follows immediately after alignment or is scheduled for the next day depending on the specific instrument.

While the sample loading process benefits from automation [2], the characterization of each target remains a manual task. It involves locating individual target locations before exposure to the X-ray source.

The solid sample scanner workflow of the HED instrument has undergone significant improvements, including pre-characterization of samples prior to beam time and the creation of a dedicated database for storing sample-related data. In this paper, we provide a comprehensive overview of the enhancements and automation implemented within the workflow, demonstrating the effectiveness of these improvements.

WORKFLOW AUTOMATION

The fundamental workflow has remained largely unchanged; however, significant modifications have been introduced with the aim of automating, standardizing, and accelerating the process of illumininating multiple targets located in one sample. An overview is presented in Fig. 1.

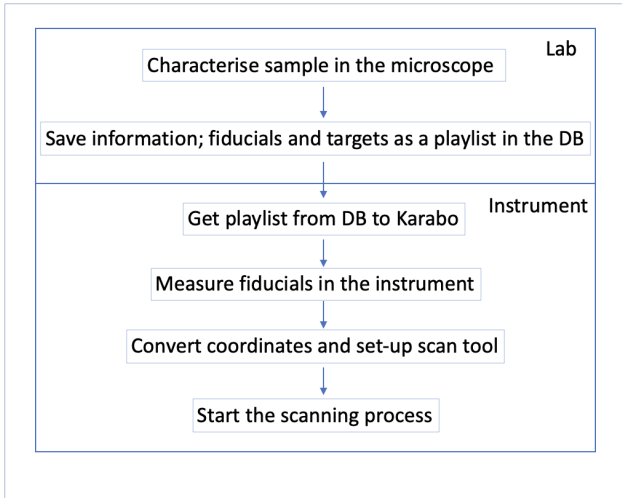

Figure 1: Workflow schema follow during sample scanner after automation.

In the updated workflow, several modifications have been implemented to streamline and expedite the process:

- Target localization before the beam time: targets are located in the sample environment and characterization labs before the experiment. Due to the addition of reference marks, fiducials, to the sample, the targets coordinates can be measured in the lab and then used at the instrument.

* ana.garcia-tabares@xfel.eu

ISBN: 978-3-95450-238-7 ISSN: 2226-0358 doi:10.18429/JACoW-ICALEPCS2023-M02A003

- Database Integration: target and fiducial coordinates are stored in a relational database for easy access and management.
- Seamless control system integration: information is directly accessible via the Karabo [4] control system, enhancing real-time monitoring and control.
- Fiducial measurements and coordinate transformation: fiducial measurements are performed, and target coordinates are transformed from the laboratory coordinate system to the instrument system. Further information can be found in the EXPERIMENTAL SETUP and in APPENDIX A.
- Streamlined coordination: transformed coordinates are subsequently transmitted to the Karabo scan tool [5], facilitating efficient sample measurement.

EXPERIMENTAL SETUP

Sample

Solid samples include designated targets and fiducial marks; fiducial marks serve as the essential navigational aids within the revised workflow system. They enable the transportation of samples between different locations, such as from the laboratory to the instrument, without the need to measure target positions again.

Prior to the experiment, the fiducial positions are established through a preliminary investigation procedure utilizing optical microscopy, specifically, a combination of 2D and 3D microscopy techniques [1].

The solid samples used during a commissioning experiment, shown in Fig. 2, were $25 \times 50\,\mathrm{mm}^2$ Si Chip with $200 \times 200\,\mu\mathrm{m}^2$ SiN membranes, containing both targets and fiducials.

For the first commissioning measurements, both fiducials and targets were fabricated through a focused ion beam (FIB), either eroded by a Ga beam for reflection geometry or created using Pt deposition on membranes to produce shadows in a transmission geometry.

Each target was uniquely identified by a cross and an incremental number. To determine the positions of these features accurately in three-dimensional space, a confocal microscope was employed, and the resulting data was recorded and input into a database.

In the fabrication process, three fiducial crosses were created and utilized as reference points. One of these crosses functions as the origin, while the X-axis and Y-axis are defined relative to the origin by one additional fiducial, respectively. The Z-axis is subsequently generated based on the established X- and Y-axes, with perpendicular orientation to both, with a fixed length of 1mm.

Instrument

The initial experiments were conducted at the High Energy Density (HED) instrument (as shown in Fig. 3), utilizing the existing infrastructure within Interaction Chamber 1 (IC1) as described in [2, 6].

IC1 houses the Fast Solid Sample Scanner [7], it has a maximum speed of 20 mm/s and a minimum resolution of less than 2 µm, as detailed in [3, 6]. The imaging system available within IC1 employs two in-line microscopes, utilizing stereo imaging techniques for the measurement of fiducial positions. Furthermore, a high-magnification in-line microscope facilitates the examination of both samples and their support structures, as described in [6].

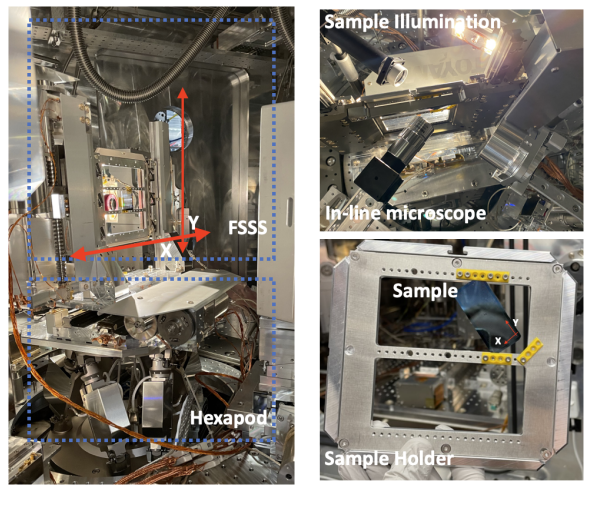

Figure 3: Instrument configuration at HED instrument.

SOFTWARE (DB AND KARABO INTEGRATION)

DB Integration

After characterizing the sample, the sample information is subsequently uploaded into a relational database. This database is comprised of multiple interconnected tables storing facility details, fiducial and target data (coordinates), as well as metadata including sample information and creation date.

Karabo Integration

An important part of the automation implementation is the connection of the database with the scan tool, and the lab coordinate transformation of lab (microscope) to the instrument system. Integrating the target coordinates into the existing "Scan Tool" at European XFEL requires several steps:

1. Access to the DB data from Karabo.
2. Coordinate transformation: this step focuses on translating coordinates between the laboratory, defined by the microscope coordinate system, and the instruments, defined by the FSSS coordinate system, taking into account the Z-axis defined by the hexapod. With this

ISBN: 978-3-95450-238-7 ISSN: 2226-0358 doi:10.18429/JACoW-ICALEPCS2023-M02A003

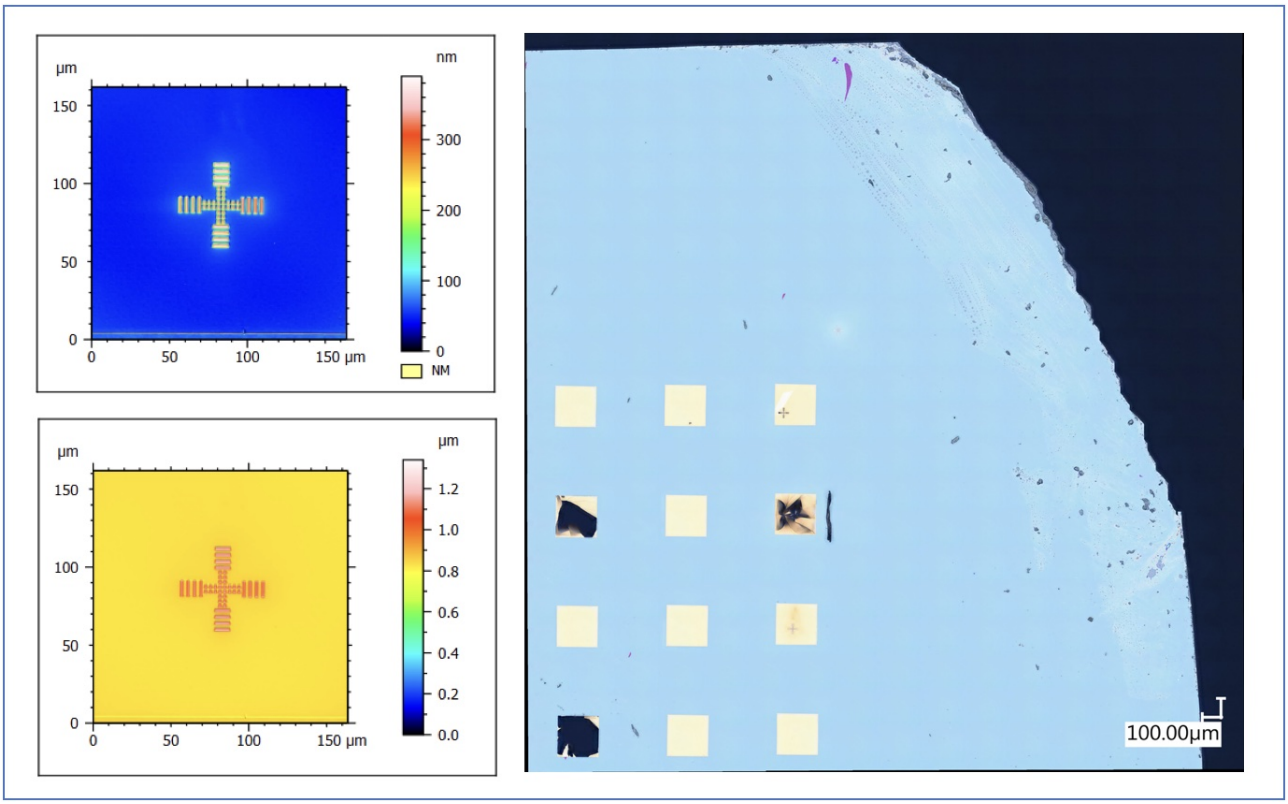

Figure 2: Sample zoom to the fiducial markers used during the first experiment.

coordinate transformation, we aim to address two potential effects: different orientations and varying image scaling due to the use of different magnification lenses in the lab and the instrument. Please refer to the APPENDIX for detailed information.

After the transformation, the target coordinates are automatically sent to the scan tool [8]. The Karabo integration also includes a graphical interface that guides the user through the workflow, making it easier to control the process (see Fig. 4).

RESULTS

During a commissioning experiment, we tested the newly introduced workflow steps, which included data retrieval from the database, coordinate transformation, the transfer of information to the scan tool and test scanning. All the steps described in the previous section were successfully validated during this commissioning experiment.

Target Accuracy

Tables 1 and 2 summarize the achieved accuracy for each of the four measured targets, highlighting variations in accuracy across the different targets. This accuracy relies on the specific target coordinates, as explained in the APPENDIX. Deviations from the current target positions are also visible in Fig. 5.

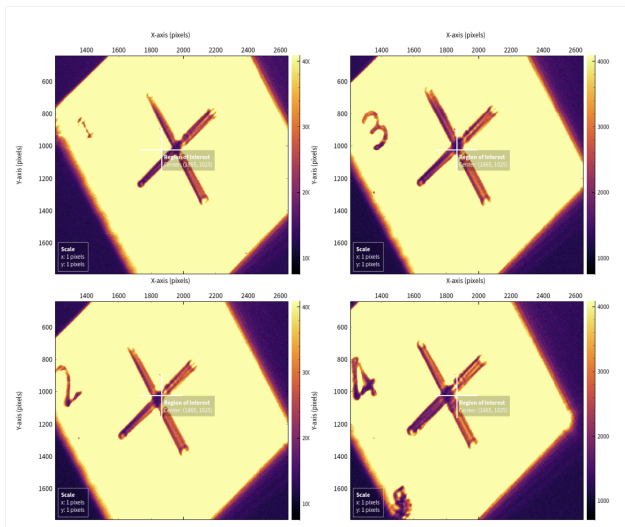

Figure 5: Target positions measured at the instrument.

Time

In Fig. 6, specifically within the "Fiducial Measurement" section of the graph, one can observe that the process of measuring fiducial positions and acquiring target coordinate positions typically takes about 30 minutes. Additionally, it's important to note that during this testing session, approx-

ISBN: 978-3-95450-238-7 ISSN: 2226-0358 doi:10.18429/JACoW-ICALEPCS2023-MO2A003

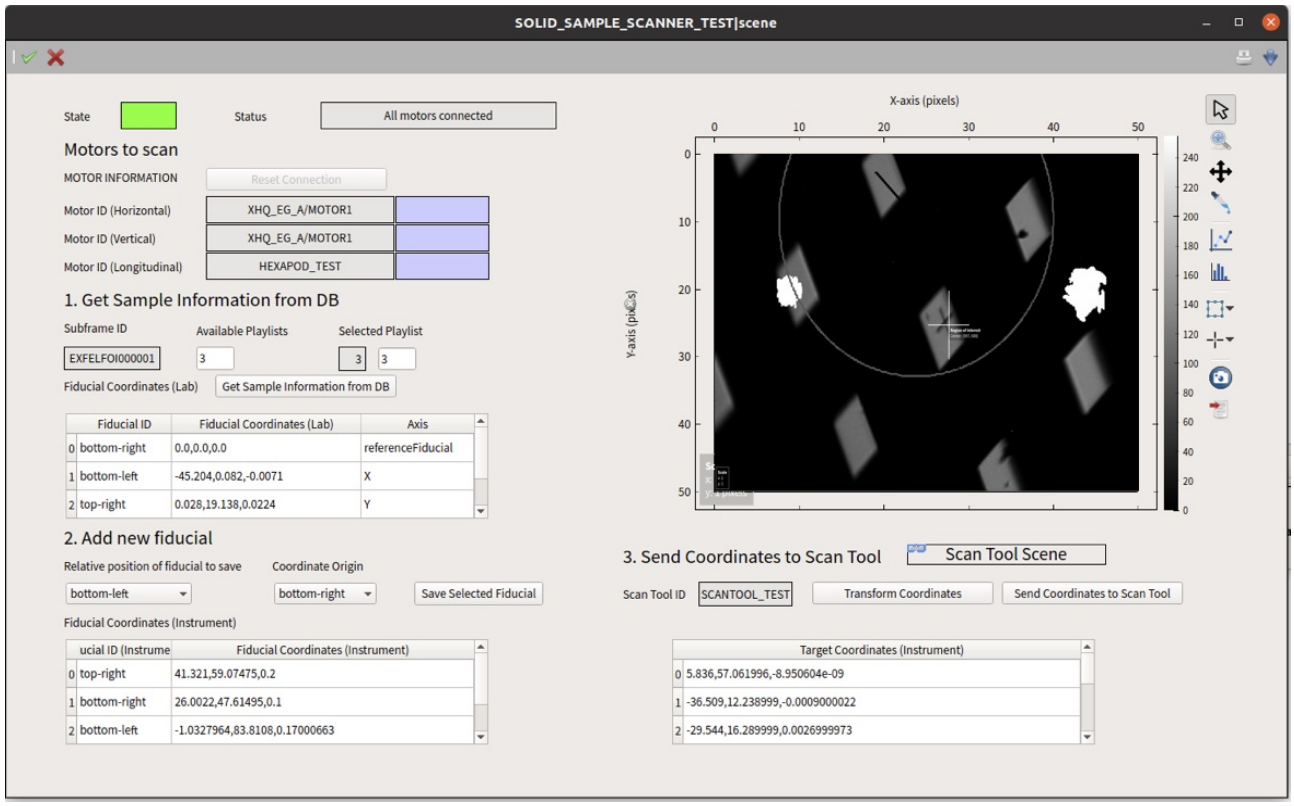

Figure 4: Auto generated scene for automatizing sample.

Table 1: Discrepancies Observed Between Estimated Target Positions and Actual Values (Horizontal Plane)

Target number	Absolute difference [µm]	Relative difference [%]
1	≈ 13	≈ 0.09
2	≈ 8	≈ 0.04
3	≈ 4	≈ 0.02
4	≈ 6	≈ 0.02

Table 2: Discrepancies Observed Between Estimated Target Positions and Actual Values (Vertical Plane)

Target number	Absolute difference [µm]	Relative difference [%]
1	≈ 6	≈ 0.007
2	≈ 3	≈ 0.004
3	≈ 5	≈ 0.007
4	≈ 6	≈ 0.01

imately 25 extra minutes were dedicated to the thorough verification of the target positions.

CONCLUSIONS

Automation within the solid sample scanner is instrumental in achieving faster and more efficient operations and data management.The automated procedures have significantly expedited tasks, leading to faster and more efficient operations. Including a precharacterization step for the samples can optimize beam time use substantially, reducing the time by 4 to 8 hours compared to the existing manual procedure. This not only saves costs but also enhances efficiency. The allocated beam times are typically 5-6 days, with 4-5 days for measurements, making the impact considerable.

The results of the calculation of the positions of the four targets within the sample were found to be remarkably accurate. The average precision achieved was 8 µm in the horizontal plane and 5 µm in the vertical plane, which reflects an average relative precision of less than 0.05%. The achieved precision is largely influenced by the accuracy of fiducial measurements performed both in the laboratory and at the instrument, as well as the precise determination of target coordinates in the laboratory, as elaborated in the appendix. To further improve the accuracy level, a combination of manual and automatic target locations can be utilised.

ISBN: 978-3-95450-238-7 ISSN: 2226-0358 doi:10.18429/JACoW-ICALEPCS2023-M02A003

Figure 6: Historical values from the commissioning day displayed in Grafana.

Furthermore, the integration of the scanner into the facility's control system, Karabo, has been succesfully tested. This integation further streamlines and accelerates the entire process, not only providing easier access to experimental data but also simplifying the operation for the instrument scientist.

Finally, data accessibility has been improved, the system now enables access to historical data values, as illustrated in Fig. 6.

APPENDIX

Fiducials vector coordinates are measured in two bases, lab and instrument. In both cases, the basis, B, is:

$$B = \begin{bmatrix} 1 & 0 & 0 \\ 0 & 1 & 0 \\ 0 & 0 & 1 \end{bmatrix}$$

In the process, two coordinate transformations are required to obtain the target coordinates in the instrument basis, i.e. the coordinates that will be used with the sample scanner.

- Base transformation from sample to lab: The change of the basis matrix -or transition matrix- from Sample basis (S) to Lab basis (L) is the one whose columns are the coordinates vector of S with respect to L. In this matrix, shown in Eq. (1), F_1 and F_2 correspond to the coordinates of Fiducials 1 and 2, as measured in the lab base, while N_x, N_y, and N_z represent the normal vector perpendicular to the sample plane.

A basis is defined using the coordinates of fiducials measured in the lab, and target coordinates are transformed to this basis (sample). To perform this coordinate transformation, we utilize the inverse of the base transformation from sample to lab, L.

$$\begin{bmatrix} T_{x,s} \\ T_{y,s} \\ T_{z,s} \end{bmatrix} = \begin{bmatrix} F_{1,x} & F_{2,x} & N_{1,x} \\ F_{1,y} & F_{2,y} & N_{1,y} \\ F_{1,z} & F_{2,z} & N_{1,z} \end{bmatrix}^{-1} \begin{bmatrix} T_{x,l} \\ T_{y,l} \\ T_{z,l} \end{bmatrix} \quad (1)$$

- Base transformation from sample to instrument The change of the basis matrix -or transition matrix- from Sample basis (S) to Instrument basis (I) is the one whose columns are the coordinates vector of S with respect to I. After the sample has been transported to the instrument, we re-measure the fiducials in the instrument's reference frame. Subsequently, we calculate the sample-instrument matrix, I, as demonstrated in Eq. (2).

  In this equation, F_1 and F_2 denote the coordinates of Fiducials 1 and 2 as measured in the instrument's reference frame with respect a third Fiducial 3 ($\vec{O}$) chosen as the coordinate origin, e.g. $\vec{F_1'} = \vec{F_1} - \vec{O}$, while N_x, N_y, and N_z represent the normal vector to F_1 and F_2 in the direction of the beam.

$$I = \begin{bmatrix} F'_{1,x} & F'_{2,x} & N_{1,x} \\ F'_{1,y} & F'_{2,y} & N_{1,y} \\ F'_{1,z} & F'_{2,z} & N_{1,z} \end{bmatrix} \quad (2)$$

ISBN: 978-3-95450-238-7 ISSN: 2226-0358 doi:10.18429/JACoW-ICALEPCS2023-MO2A003

- Additionally, an scaling factor, S, is computed to compensate any magnification discrepancies between the instrument and the lab optical system.

$$S = \frac{\sqrt{F'_{i,x,l} + F'_{1,y,l} + F'_{i,z,l}}}{\sqrt{F'_{i,x,s} + F'_{1,y,s} + F'_{i,z,s}}} \tag{3}$$

Targets coordinates are then transformed, from sample basis to instrument basis, by multiplying transformation matrix S with the the target coordinates sample T_s and adding the origin vector:

$$\overrightarrow{T_I} = S \cdot I \cdot L \cdot (\overrightarrow{T_S}) + \overrightarrow{O} \tag{4}$$

Error Propagation

The target accuracy is given by a combination of the fiducilas measurements both in the lab and in the instrument and the target measurements in the lab.

Simplifying the calculations, separating the Eq. (4) in two, $T_1 = S \cdot \overrightarrow{T_S}$ and $T_2 = \overrightarrow{O}$ the relative errorbar can be calculating as shown in Eq. (5).

$$(\sigma T_I)^2 = (\sigma T_1)^2 + (\sigma T_2)^2 \tag{5}$$

Starting with the first term, denoted as T_1, and under the assumption that the fiducial basis maintains a consistent orientation in both the laboratory and instrument settings—meaning the sample's angle with respect to the frame is approximately $\frac{n\pi}{2}$—we operate with diagonal matrices, which simplifies the error calculation.

$$\left(\frac{\sigma T_{x,y,z}}{T_{x,y,z}}\right)^2 \approx 2\left(\frac{\sigma F_{x,y,z,L}}{F_{x,y,z,L}}\right)^2 + 4\left(\frac{\sigma F_{x,y,z,I}}{F_{x,y,z,I}}\right)^2 + \left(\frac{\sigma F_{x,y,z,L}}{F_{x,y,z,L}}\right)^2 + 2\left(\frac{\sigma F_{x,y,z,I}}{F_{x,y,z,I}}\right)^2 + \left(\frac{\sigma T_{x,y,z,L}}{T_{x,y,z}}\right)^2 \tag{6}$$

This can be further simplified

$$\left(\frac{\sigma T_{x,y,z}}{T_{x,y,z}}\right)^2 \approx 3\left(\frac{\sigma F_{x,y,z,L}}{F_{x,y,z,L}}\right)^2 + 6\left(\frac{\sigma F_{x,y,z,I}}{F_{x,y,z,I}}\right)^2 + \left(\frac{\sigma T_{x,y,z,L}}{T_{x,y,z,L}}\right)^2 \tag{7}$$

Simplifying further, and assuming uniform relative errors across the board, where the accuracy of target measurements is half that of lab-based fiducials, and the accuracy of instrument-measured fiducials is one and a half times that of lab-measured fiducials.

$$\left(\frac{\sigma T_{x,y,z}}{T_{x,y,z}}\right)^2 \approx 14\left(\frac{\sigma F_{x,y,z,L}}{F_{x,y,z,L}}\right)^2 \tag{8}$$

Adding the contribution of the second term of the equation (5), we obtain an approximate error calculation

$$\sigma {T_{x,y,z}}^2 \approx 14\left(T_1\frac{\sigma F_{x,y,z,L}}{F_{x,y,z,L}}\right)^2 + 1.5\sigma {F_{x,y,z,L}}^2 = \sigma F^2_{x,y,z,L}\left(14\left(\frac{T_1}{F_{x,y,z,L}}\right)^2 + 1.5^2\right) \tag{9}$$

Depending on the ratio $\frac{T_1}{F_{x,y,z,L}}$, we observe error bars that vary between two to seven times the fiducial lab error bars. For instance, with a 1.5 µm error bar, the target error can range from 3 µm to 10.5 µm, aligning with the findings reported in the "RESULTS" section.

REFERENCES

[1] C. Deiter, "Status of the procedures for fixed-targets at the C. Deiter instruments of the European XFEL", Users meeting 2023.

[2] M. Makita *et al.*, Sample stage at the HED: mount design and exchange system in vacuum: Standardized sample holder concept and load-lock exchange system.

[3] Ulf Zastrau, "The HED Instrument at the European XFEL, HED-HiBEF satellite meeting to the EuXFEL/DESY UM 2020", EuXFEL, Germany, January 28th, 2020, https://www.xfel.eu/sites/sites_custom/site_xfel/content/e35165/e46561/e46886/e46963/e127531/xfel_file127533/210120_Appel_HEDHIBEF_UM_satellite_v1.0_web_eng.pdf

[4] Steffen Hauf *et al.*, "The Karabo distributed control system", *J. Synchrotron Radiat.*, vol. 26, pp. 1448–1461, 2019. doi:10.1107/S1600577519006696

[5] Scan Tool documentaion, https://rtd.xfel.eu/docs/scantool/en/latest/introduction.html

[6] Ulf Zastrau *et al.*, "The High Energy Density Scientific Instrument at the European XFEL", *J. Synchrotron Radiat.*, vol. 28, pp. 1393–1416, 2021. doi:10.1107/S1600577521007335

[7] Carsten Deiter, "The Fast Solid Sample Scanner for SCS", Hamburg, 2017, https://www.xfel.eu/sites/sites_custom/site_xfel/content/e51499/e60513/e63558/e107746/e63567/e63596/6_XFUM2017-SASE3_Satellite_SCS_Deiter_Sample_environment_eng.pdf

[8] Ivars Karpics, "Current and future developments of European XFEL scan tool Karabacon", in *NOBUGS 2022*, Paul Scherer Institute, Villigen, Switzerland, 2022, https://indico.psi.ch/event/12738/contributions/38938/